Title

Trb3 controls mesenchymal stem cell lineage fate and enhances bone regeneration by scaffold-mediated local gene delivery

Authors

Fan, Jiabing
Lee, Chung-Sung
Kim, Soyon
et al.

Publication Date

2021

DOI

10.1016/j.biomaterials.2020.120445

Peer reviewed

HHS Public Access

Author manuscript

Biomaterials. Author manuscript; available in PMC 2022 January 01.

Published in final edited form as:

Biomaterials. 2021 January ; 264: 120445. doi:10.1016/j.biomaterials.2020.120445.

Trb3 Controls Mesenchymal Stem Cell Lineage Fate and Enhances Bone Regeneration by Scaffold-Mediated Local Gene Delivery

Jiabing Fan[1,2], **Chung-Sung Lee**[1], **Soyon Kim**[1], **Xiao Zhang**[1], **Joan Pi-Anfruns**[3], **Mian Guo**[4], **Chen Chen**[1], **Matthew Rahnama**[1], **Jiong Li**[5], **Benjamin M. Wu**[1,2,6], **Tara L. Aghaloo**[3], **Min Lee**[1,2,6,*]

[1]Division of Advanced Prosthodontics, School of Dentistry, University of California, Los Angeles, California, 90095, USA

[2]Weintraub Center for Reconstructive Biotechnology, School of Dentistry, University of California, Los Angeles, California, 90095, USA

[3]Division of Diagnostic and Surgical Sciences, School of Dentistry, University of California, Los Angeles, California, 90095, USA

[4]Department of Neurosurgery, the 2nd Affiliated Hospital of Harbin Medical University, Harbin, Heilonjiang, 150001, China

[5]Department of Medicinal Chemistry, Institute for Structural Biology, Drug Discovery and Development, Philips Institute for Oral Health Research, Virginia Commonwealth University, Richmond, Virginia, 23298, USA

[6]Department of Bioengineering, University of California, Los Angeles, California, 90095, USA

Abstract

Aberrant lineage commitment of mesenchymal stem cells (MSCs) in marrow contributes to abnormal bone formation due to reduced osteogenic and increased adipogenic potency. While several major transcriptional factors associated with lineage differentiation have been found during the last few decades, the molecular switch for MSC fate determination and its role in skeletal regeneration remains largely unknown, limiting creation of effective therapeutic approaches. Tribbles homolog 3 (Trb3), a member of tribbles family pseudokinases, is known to exert diverse roles in cellular differentiation. Here, we investigated the reciprocal role of Trb3 in the regulation of osteogenic and adipogenic differentiation of MSCs in the context of bone formation, and examined the mechanisms by which Trb3 controls the adipo-osteogenic balance. Trb3 promoted osteoblastic commitment of MSCs at the expense of adipocyte differentiation. Mechanistically, Trb3 regulated cell-fate choice of MSCs through BMP/Smad and Wnt/β-catenin signals. Importantly, *in vivo* local delivery of Trb3 using a novel gelatin-conjugated caffeic acid-coated

*To whom correspondence should be addressed: Min Lee, PhD, Professor, Division of Advanced Prosthodontics, Weintraub Center for Reconstructive Biotechnology, Department of Bioengineering, University of California, Los Angeles, 10833 Le Conte Ave., Box 951668, Los Angeles, CA, 90095, Phone: 310-825-6674, Fax: (310) 825-6345, leemin@ucla.edu.

Competing interests statement

The authors indicated no potential conflicts of interest.

apatite/PLGA (GelCA-PLGA) scaffold stimulated robust bone regeneration and inhibited fat-filled cyst formation in rodent non-healing mandibular defect models. These findings demonstrate Trb3-based therapeutic strategies that favor osteoblastogenesis over adipogenesis for improved skeletal regeneration and future treatment of bone-loss disease. The distinctive approach implementing a scaffold-mediated local gene transfer may further broaden the translational use of targeting specific therapeutic gene related to lineage commitment for clinical bone treatment.

Keywords

Trb3; MSC; Osteogenesis; Adipogenesis; GelCA-PLGA Scaffold

1. Introduction

Non-healing bone injuries are an increasing source of patient morbidity and remain an important medical challenge, affecting millions of people worldwide (1,2). In addition, population aging increases the prevalence of osteoporosis, a systemic bone disease characterized by reduced bone mass and an increased risk of fracture (3). The growing medical burden of bone diseases facilitates the development of effective therapeutic strategies for bone regeneration.

Mesenchymal stem cells (MSCs) are multipotent cells that can differentiate into mature cells of mesenchymal tissues such as fat and bone (4). MSCs as a common progenitor of osteoblast and adipocyte are delicately balanced for their fate commitment (4). New bone formation and adult skeletal homeostasis are attributed to the reciprocal regulation of MSCs in their osteogenic and adipogenic lineage commitment (5). The dysregulation of the adipo-osteogenic differentiation of MSCs in marrow may lead to osseous abnormalities and bone diseases (6). Pathologic conditions in osteoporosis increase MSC commitment toward an adipogenic lineage at the expense of osteoblastic differentiation, resulting in increased marrow fat accumulation and reduced bone mass (6–8). Modulating the balance between adipogenesis and osteogenesis thus poses a promising alternative strategy for improved skeletal regeneration. Such strategy also presents potentials for an alternative anabolic therapy for prevention and treatment of osteoporotic-related bone loss.

The transcriptional control of MSC lineage commitment is strictly regulated by various molecular factors and signals (9). Differentiation of MSCs into osteoblasts and adipocytes has been found to be orchestrated by two key transcriptional factors, Runx2 and PPARγ (9,10). MSCs primed to a certain cell lineage may be further regulated by molecular cues within the local bone marrow microenvironment (11). Abnormally stimulated or aged MSCs revealed a preference to adipocyte differentiation rather than osteoblast differentiation (12,13). Identification of specific molecular switches that govern MSC lineage commitment is extraordinarily crucial to the creation of efficacious therapeutic approaches that combat the aberrant lineage commitments associated with abnormal skeletal regeneration and pathological osteoporotic diseases (14).

Tribbles homolog 3 (Trb3) is a member of tribbles family pseudokinases that exhibits crucial metabolic functions in various tissues, as well as essential roles in cellular differentiation by

regulating activity of various transcriptional factors (15–19). A previous study indicates that Trb3 plays an important role in regulating bone morphogenetic protein (BMP) signaling (20). Our recent studies showed that small molecule drug-induced Trb3 stimulated osteoblastic differentiation of adipose-derived stem cells and *in vivo* bone formation (21,22). In addition, Trb3 was previously revealed to suppress lipid synthesis via degrading an acetyl coenzyme A (a rate-limiting enzyme for fatty acid synthesis) (15), and suppressed adipocyte differentiation in pre-adipocytes through negatively regulating PPARγ transcriptional activities (23). These observations suggest that Trb3 is a promising molecular target to regulate adipo-osteogenic differentiation of MSCs. No studies have explored the direct roles of Trb3 in the reciprocal regulation between osteogenic and adipogenic mesenchymal cell differentiation in the context of bone regeneration. Moreover, the mechanisms by which Trb3 controls the adipo-osteogenic balance are unknown. Taken together, upregulation of Trb3 by gene transfer may favor osteogenic lineage commitment of MSCs over an adipogenic lineage, providing promising treatment options to improve bone repair.

Biomaterial scaffolds provide a versatile platform for localized and efficient gene delivery in therapeutic applications. A wide variety of approaches to immobilize gene therapy vectors onto the scaffold surface have been developed to ensure that the vectors stay concentrated in the defective areas and confer long-term transgene expression (24–28). We have previously demonstrated that PLGA scaffolds with apatite coatings (Ap-PLGA) served favorable substrates to deliver bioactive agents for bone regeneration in various defect models (29–32). However, such delivery approach through non-specific physical adsorption may be easily affected by surrounding environments and lead to premature burst release with low binding affinity *in vivo*, requiring further modifications to enhance surface binding. Recently, catechol chemistry has been employed to immobilize biomolecules onto scaffold surfaces in a simple and effective manner due to the ability of catechol moieties to adhere to a wide range of organic or inorganic substrates and serve as linkers between the immobilizing surfaces and the biomolecules (33–36). Gelatin is hydrolyzed collagen, a main structural protein in bone tissue, and has been an attractive biopolymer for bone tissue engineering due to its many desirable properties including good biocompatibility, low immunogenicity, cell adhesion, and easy of gelation (37–40). Thus, gelatin modified with catechol containing molecules such as caffeic acid can be layered onto Ap-PLGA scaffolds for enhanced gene delivery.

In this study, we found that Trb3 acted as a key molecular switch determining MSC lineage fate by regulating adipogenesis and osteogenesis programming. Mechanistic studies further illustrated that Trb3 controlled cell-fate choice of MSCs via cooperative activation of BMP/Smad and Wnt/beta-catenin signals, two major signals governing skeletal development and bone formation. Moreover, local delivery of Trb3 through the creation of a novel gene-activated hybrid scaffold significantly promoted bone regeneration and inhibited fat-filled bone void formation in a clinically related rodent mandibular defect model. These findings offer new insights of molecular regulation on the lineage commitment of MSCs, and specifically targeting a molecular switch that controls adipocyte-osteoblast lineage commitment may be a novel therapeutic alternative for bone defect repair and bone-loss related disease treatment.

2. Materials and Methods

2.1 Cell culture and transduction

Human MSCs (hMSCs) (Lonza, Vancouver) were grown in human MesenCult™ medium (STEMCELL Technologies, Vancouver). For overexpression of Trb3, cells were transfected by lentivirus particles encoding Trb3 (Vectorbuilder, IL) or plasmid-expressed Trb3 using lipofectamine 2000 (Invitrogen). To knockdown Trb3, cells were transfected by Trb3 siRNA or lentivirus particles containing shRNA targeting Trb3 (Santa Cruz Biotechnology, CA). hMSCs collected from four different patients were used for experiments. Mouse MSCs (mMSCs) (D1 ORL UVA, ATCC, VA) were grown in DMEM (Invitrogen, CA) supplemented with 10% FBS and used to validate the efficacy of gene-loaded scaffolds before *in vivo* testing.

2.2 ALP activity, Alizarin red stain, Adipored assay and Oil red stain

To assess the degree of osteogenic differentiation, MSCs were grown in osteogenic medium (OM, Sigma, MO) containing 50 μg/mL L-ascorbic acid, 10 mM β-glycerophosphate and 100 nM dexamethasone. For detecting alkaline phosphatase (ALP) expression, cells was induced at indicated times, fixed with 10% formalin, and stained with ALP colorimetric kit (Sigma) containing 5-Bromo-4-chloro-3-indoxylphosphate, Nitro Blue tetrazolium, and AP buffer. To quantitatively measure ALP activity, cells were digested in NP-40 lysis buffer (Life technologies, CA), incubated in the buffer containing p-nitrophenol phosphate substrate (Sigma) by measurement of absorbance at 405 nm, and normalized with whole DNA content detected by PicoGreen dsDNA kit (Life technologies). To detect mineral deposition, cells were stained with 2% alizarin red solution (Sigma). The stained cells were further quantitatively measured by dissolving the stained cells in 10% (v/v) acetic acid with measurement of absorbance at 405 nm. For adipogenic differentiation, cells were grown in adipogenic medium (Sigma) containing 250μM 3-Isobutyl-1-methylxanthine (IBMX), 200 μM indomethacin and 0.1 μM dexamethasone. Intracellular lipid accumulation of cells was assessed through an Adipored kit (Lonza) with absorbance at 572 nm, and stained with 0.2% Oil Red O solution (Sigma).

2.3 RNA extraction, Real-time PCR, and RNA-Seq

Total RNA was extracted from the cells by Trizol reagent (Life Technologies) and RNeasy Mini kit (Qiagen, CA) according to the manufacture's protocol. A 500 ng aliquot of RNA in each sample was adopted to synthesize complementary DNA using a SuperScript III First-Strand Synthesis System (Life Technologies). Real-time PCR analysis was conducted with a 20 μL of SYBR Green reaction system in a LightCycler 480 PCR instrument (Roche, IN). GAPDH was used as an internal control to normalize the expression level of each target gene. All primer sequences were listed in Table S1. To examine cell gene expression profile, high-throughput RNA-Seq was performed at the UCLA sequencing core facilities. RNA-seq libraries were prepared by KAPA RNA-Seq Library Preparation Kits (KAPA Biosystems, IN). The pooled libraries were subsequently sequenced by an Illumina HiSeq 3000 machine. GSEA was used to analyze the set of gene signatures related to signaling pathways. The heatmap was further generated with Morpheus.

2.4 Immunoprecipitation and western blotting

Cells were washed with PBS, harvested, and lysed in 0.2% NP-40 lysis buffer. The protein lysates were subjected to immunoprecipitation with antibodies containing anti-Smad4 or anti-β-catenin (Abcam, MA) overnight, and then incubated with protein A/G Plus Agarose (Fisher) for 4 hours. The immunocomplex was washed with PBS three times, followed by mixture with SDS buffer. For western blotting, whole cell or co-precipitated extracts were separated by a Sodium Dodecyl Sulfate-Polyacrylamide Gel Electrophoresis (SDS-PAGE), blotted onto Immobilon polyvinyl difluoride (PVDF) membrane (Millipore, MA), and incubated with primary antibodies containing anti-Trb3, anti-Smad4, anti-β-catenin or anti-GAPDH. The membranes were subsequently incubated in secondary antibodies conjugated with Horseradish Peroxidase (HRP) (Millipore, MA) and visualized with chemiluminescent HRP (Denville Scientific, NJ).

2.5 Chromatin immunoprecipitation (ChIP) assay

ChIP assay was carried out using a ChIP assay kit (Millipore, MA) according to the manufacturer's instructions. Briefly, cells were washed with PBS and cross-linked with 1% formaldehyde (Sigma) for 10 min. Precipitated DNA samples were quantified with real-time RCR, and data was presented as the percentage of input DNA. Antibodies for ChIP assay included anti-Smad4, anti-β-catenin, and negative anti-IgG. Primer sequences were listed in Table S2.

2.6 Immunofluorescence (IF) staining

Cells were fixed in 4% paraformaldehyde, subjected to permeabilization with PBS solution containing 2% Triton X-100 and incubated with the primary antibodies including anti-Trb3 and anti-Smad4 or anti-β-catenin. Cells were further treated with the mixture of two secondary antibodies (Anti-rabbit FITC and Anti-goat Texas red). For counter stain, cells were incubated with Hoechst 33342. Fluorescence images were detected by a confocal laser scanning microscopy (LSM 880, Zeiss, Germany). For paraffin-embedding tissues, the primary antibodies containing anti-pSmad1/5/8 or anti-LEF1 were used.

2.7 Transduction assay of AAV serotypes *in vitro*

mMSCs were seeded in 12-well plates at density of 3×10^4 cells per well. After 24 hours, cells were respectively incubated with 6 different EGFP-encoded AAV particles (AAV1, AAV2, AAV5, AAV6, AAV8, AAV9) (Vectorbuilder) at titer of 1×10^{11} GC/ml. After 48 hours post-incubation, EGFP expression was visualized with an Olympus IX71 microscope (Olympus, Japan). Protein expression of EGFP was further assessed by an immunoblotting assay with an anti-GFP antibody. Lastly, AAV2-encoding full-length Trb3 was used to treat mMSCs, and Trb3 expression was measured by immunoblotting assay with an anti-Trb3 antibody.

2.8 Gelatin-conjugated caffeic acid (GelCA) synthesis

GelCA was synthesized though a standard EDC chemistry. Gelatin (4.0g, Sigma) was dissolved in distilled water/DMSO (5:2, 70 mL, pH 5). Caffeic acid (2.44 mg), EDC (514 mg), and NHS (308 mg) were dissolved in DMSO (10 mL) and added to the gelatin

solution. The pH of the solution was adjusted to 4.5 to prevent the oxidation of catechol groups. After reacting overnight, the product was purified by membrane dialysis (MWCO: 3,500, Spectra/Por®, CA) against pH 4.0 deionized water for 2 days and deionized water for 4 h and then was freeze dried.

2.9 PLGA preparation and surface coating

PLGA scaffold was fabricated via the process of solvent casting and leaching methods. PLGA/chloroform solution was blended with sucrose (200–300 μm diameter) to generate a porosity of around 92% (volume fraction), compressed into a Teflon mold, and undergone with a vacuum freeze-dry overnight at 100 mTorr and −110 °C (SP Industries, Inc., PA). The scaffolds were subsequently washed with distilled water to remove sucrose and disinfected in 70% ethanol. The scaffold sheets were cut into small plates with appropriate size. PLGA plates were first coated with an apatite layer through process of simulated body fluid (SBF) incubation. The surface of the apatite/PLGA was subsequently subject to GelCA coating to form GelCA-PLGA scaffold: apatite/PLGA scaffold was immersed into 0.2% or 1% GelCA solution with 0.05% sodium periodate (Sigma) overnight at 37 °C.

2.10 Characterization of GelCA-coated scaffolds

Nuclear magnetic resonance (NMR) spectroscopy (Bruker Avance, 400 MHz, D_2O) was used to confirm the conjugation of caffeic acid to gelatin. The morphology of scaffolds was observed by a scanning electron microscopy (SEM) (Nova NanoSEM 230, FEI, OR). The elemental composition of scaffolds was evaluated using Energy-dispersive X-ray (EDX) spectroscopy. Apatite formation and GelCA coating on the scaffolds were further verified by Fourier-transform infrared (FTIR) spectroscopy (Jasco 420). The compressive modulus of scaffolds was measured by Instron Electro-Mechanical Testing Machines (Instron, Model 5564, Norwood, MA) using a flat-ended indenter (1.6 mm in diameter).

2.11 Gene and protein release kinetics

To measure the release kinetics of gene and protein from scaffold, AAV particles (5×10^{11} GC, Vectorbuilder) and rhBMP-2 (2μg, R&D system, MN) was respectively mixed with GelCA solution, and layered onto Apatite/PLGA scaffold overnight at 37 °C. The gene or protein-loaded scaffolds were immersed in 1 mL of PBS in the absence or presence of 1 unit mL^{-1} collagenase type II (Sigma) at 37°C, and the incubating solution was removed and replaced with 1 mL of fresh PBS solution at predetermined time points over 7 days, analyzed by a qPCR AAV Titration Kit (abm, Canada) and a quantikine BMP-2 ELISA kit (R&D system), respectively.

2.12 Interaction of cell, AAV and scaffold

Mouse MSCs (5×10^6 cells/ml) and EGFP-encoded AAV particles (5×10^{11} GC) were mixed with pheophorbide A-encapsulated GelCA and layered onto the apatite/PLGA scaffold. After 3 days, the cells were treated with Hoechst for 30 min to stain the nuclei. After incubation, the medium was removed, and the cells were rinsed twice with PBS. Cell/scaffold were observed using a confocal laser scanning microscopy (LSM 880). Uptake

efficiency (%) of cells was also obtained by a flow cytometry (BD LSRFortessa X-20 SORP, Becton Dickinson, CA).

2.13 Cell differentiation on hybrid scaffold

To assess cell proliferation on the scaffolds, mMSCs (5×10^6 cells/ml) were mixed with GelCA solution, layered onto apatite/PLGA scaffolds, stained with a Live/Dead staining kit (Life Technologies) for 15 minutes, and imaged under an Olympus IX71 microscope at days 1, 7, and 14. To quantify cell proliferation, the cell/scaffold complex was analyzed with the AlamarBlue assay kit (Life Technologies). For measuring osteogenic differentiation, GelCA encapsulated with AAV-Trb3 and mouse MSCs was coated onto Apatite/PLGA scaffold, cultured with OM and measured by ALP staining and activity at days 7 and 14.

2.14 Rodent craniofacial bone defect models

Animal surgery was carried out in these studies according to protocols approved by the UCLA Animal Research Committee and was strictly in compliance with the Guidelines for the Care and Use of Laboratory Animal of the National Institutes of Health. Calvarial defect model was created in CD-1 nude mice (male, 8–10 weeks old, Charles River) for hMSC implantation. Calvaria of mice underwent a trephine drill with constant irrigation and 3-mm full-thickness craniotomy defects were established in each parietal bone without injuring underlying dura mater. Apatite/PLGA scaffolds alone or seeded with hMSCs with Trb3 overexpression or control (1×10^7 cells/ml) were implanted into calvarial defects (6 mice/group). Critical-sized mandible defects were created in Sprague Dawley rats (male, 8–12weeks, Charles River) to examine the direct effect of Trb3 *in vivo*. After animals underwent general anesthesia via inhalational isoflurane, an incision that overlies and parallels the left mandible was created using a size of No. 15 blade with a sterile manner. The inferior border of the mandible was identified when deepening down via subcutaneous tissues, and the major mandible body was subsequently exposed after splitting the pterygomasseteric sling using electrocautery. A 1-mm high-speed cutting burr was applied to precisely drill a 5 × 5 mm defect with constant copious irrigation. A GelCA-PLGA scaffold loaded with AAV-Trb3 (2.5×10^{11} GC, 2.5×10^{12} GC) or/and BMP2 (30 μg) was then placed onto the mandibular defect (6 rats/group). All surgical animals were allowed to fully recover from anesthesia on a warm sheet and were then transferred to the vivarium for postoperative care. All animals got analgesia via subcutaneous injections of 0.1mg/kg buprenorphine for 3 days postoperatively and received drinking water containing trimethoprim–sulfamethoxazole for 7 days to prevent potential infection.

2.15 Microcomputerized tomography scanning

Animals were sacrificed at the indicated times post-implantation. Harvested tissues underwent fixation with 4% formaldehyde and were stored in 70% ethanol for further imaging. High-resolution microcomputerized tomography (μCT) machine (SkyScan 1172, Belgium) set at 57 kVp, 184 μA, 0.5 mm aluminum filtration, and 10 μm resolution was used to scan samples. All data were visualized and three-dimensionally reconstructed by a Dolphin 3D software (Dolphin Imaging & Management Solutions, CA). The new bone area and volume were measured using ImageJ software (NIH) and CTAn (SkyScan), respectively.

Bone-specific analysis included new bone area/original defect area (percent area), new bone volume/total volume, and trabecular number, bone mineral density and bone thickness.

2.16 Histological and immunohistochemical analyses

The fixed tissues were decalcified in 10% ethylenediaminetetraacetic acid (EDTA), embedded in paraffin and cut into 5μm thickness of sections. The tissue sections were subsequently deparaffinized with xylene, and stained with hematoxylin and eosin (H&E) solution and Masson's trichrome kit (Sigma) to detect new bone formation visualized with light blue color. The deparaffinized slides was further stained with 0.1% Picrosirius red solution (Polysciences, PA) and imaged using a polarizing light microscope. 0.2% Oil Red O solution was also adopted to stain adipocytes. For immunohistochemical analysis, the deparaffinized sections were incubated with the primary antibodies (Santa Cruz), including anti-Trb3, PPARγ, Runx2, OCN, followed by the HRP/DAB detection kit (Abcam), and counterstaining with Mayer's hematoxylin (Abcam). The colorimetric analysis of stained sections was further conducted with ImageJ software (NIH).

2.17 Statistical analysis

Quantitative data are expressed at mean ± SD, with *$p < 0.05$, **$p < 0.01$, and ***$p < 0.001$ considered statistically significant. Sample size was determined according to the assumption that a 30% difference in the parameters is considered to be significant with an estimate of sigma of 10–20% anticipated mean. Six animals per group were used for *in vivo* studies. Parametric data were analyzed by a two-tailed Student's t-test when two groups were compared. A one-way ANOVA analysis of variance was adopted when more than two groups were compared, followed by a post hoc Tukey's test to compare the two groups. The GraphPad PRISM software (v6.0, CA) was adopted for statistical analysis.

3. Results

3.1 Trb3 controls the fate decision of MSCs

To examine the effect of Trb3 on MSC lineage commitment, we found that overexpression of exogenous Trb3 using lentivirus particles-encoding Trb3 potently induced osteogenic differentiation of hMSCs as shown by increased ALP activity and mineralization as well as induced expression of osteogenic genes including *Osterix*, *Runx2*, *ALP*, and *osteocalcin* (*OCN*) (Fig. 1a–e). In contrast, knockdown of endogenous Trb3 decreased hMSC osteogenic capacity with reduced expression of osteogenic genes including *Runx2*, *ALP* and *OCN* (Fig. 1f). Moreover, we investigated whether Trb3 inhibits adipogenic differentiation in hMSCs. We found that Trb3 overexpression significantly suppressed adipogenic differentiation of hMSCs as demonstrated by decreased oil red stain and Adipored assay (Fig. 1h,i). At the molecular level, Trb3 overexpression in hMSCs reduced expression of adipogenic genes including *PPARγ, FABP4* and *LPL* (Fig. 1g). Conversely, knockdown of endogenous Trb3 increased adipogenic differentiation of hMSCs as shown by elevated adipogenic gene expression (*PPARγ* and *LPL*) and AdipoRed assay (Fig. 1j,k).

Following the *in vitro* results, we further examined whether overexpression of exogenous Trb3 increases osteogenic commitment of hMSCs *in vivo*. Trb3 overexpression hMSCs were

seeded on Ap-PLGA scaffolds and implanted into critical-sized mice calvarial defects (Fig. 2a). The bioactivity of cell-seeded constructs was confirmed *in vitro* prior to implantation (Fig. S1). Ap-PLGA scaffolds supported proliferation of hMSCs with high cell viability, and Trb3-overpressed hMSCs significantly increased the expression of ALP and osteogenic genes when compared to control hMSCs in the scaffolds. Six weeks postoperatively, micro-CT images displayed that Trb3 overexpressed hMSCs exhibited the significantly enhanced calvarial bone healing with nearly complete bone bridges crossing the defected area (Fig. 2b). Conversely, defects treated with control overexpression hMSCs or blank scaffolds had minimal bone healing without apparent bone bridge formation (Fig. 2b). Quantification of micro-CT images further demonstrated that defects treated with Trb3 overexpressed hMSCs increased the extent of bone healing to ~75.5% and ~17.8% in new bone area and bone volume/tissue volume (BV/TV) respectively, and exhibited a significant increase in trabecular number (TN) and bone mineral density (BMD) (Figure 2c–f). The elevated bone healing was also confirmed by hematoxylin and eosin (HE) stain and Masson trichrome stain/quantification (Fig. 2g,h). Defects treated with Trb3 overexpressed hMSCs were detected with abundant new bone and thick osteoid matrix almost spanning entire defect area (Fig. 2g). In addition, immunohistochemical (IHC) stain/quantification displayed that the significantly increased expression of OCN (a protein associated to bone matrix mineralization) was detected in defects treated with Trb3 overexpression hMSCs (Fig. 2g,i). Overall, Trb3 showed robust osteogenic commitment while suppressing adipogenic differentiation, indicating that Trb3 acts as a crucial molecular switch reciprocally regulating adipocyte-osteoblast lineage commitment.

3.2 Trb3 regulates lineage commitment of MSCs by BMP/Smad and Wnt/β-catenin signals

To understand the molecular mechanisms by which Trb3 determines MSC lineage commitment, we examined gene expression profiles between hMSCs with control and Trb3 overexpression at day 2 using RNA-Seq. Gene set enrichment analysis (GSEA) indicated that both BMP and Wnt signaling are significantly increased in Trb3 overexpressed hMSCs (Fig. 3a). Heatmap analysis further displayed a clear upregulation of ligands and downstream molecules of both BMP and Wnt signals in cells with Trb3 overexpression (Fig. 3b). Furthermore, we adopted small molecule inhibitors to block BMP and Wnt signals, and tested whether Trb3-mediated MSC lineage commitment is dependent on BMP and Wnt signaling. We found that blocking both BMP and Wnt signals completely abrogated Trb3-mediated expression of osteogenic genes (*Runx2* and *ALP*), whereas blocking either BMP or Wnt signal only resulted in partial abrogation (Fig. 3c,d). Blocking BMP/Wnt or Wnt signal alone was found to fully rescue Trb3-mediated inhibition of adipogenic gene expression (*PPARγ*), while blocking BMP signal alone had no significant effect (Fig. 3e). Moreover, western-blot assay confirmed that Trb3 overexpression enhanced expression of Osterix and Runx2, both key transcriptional factors for osteogenesis, and suppressed expression of PPARγ, a major transcriptional factor for adipogenesis (Fig. 3f). These outcomes suggested that Trb3 stimulated osteoblastic differentiation through mediating both BMP and Wnt signals, and suppressed adipogenic differentiation mainly through Wnt signaling.

To further gain insights of how Trb3 regulates BMP and Wnt signal, we overexpressed or down-regulated Trb3, and screened for several transcriptional factors and key components related to BMP and Wnt signals. We found that Trb3 had a direct interaction with Smad4 or β-catenin by immunoprecipitation (IP) assay (Fig. 3g,h). Confocal images of human and mouse MSCs indicated that Trb3/Smad4 or Trb3/β-catenin could be co-localized together, and displayed nuclear translocation in response to Trb3 overexpression (Fig. 3i,l, and Fig. S2). Furthermore, we found that Trb3 enhanced the recruitment of Smad4 or β-catenin to the promoter region of Runx2 (Fig. 3j,m). Trb3 promoted the recruitment of β-catenin only to the promoter region of PPARγ (Fig. 3k,n). Collectively, Trb3 interacted with Smad4 and β-catenin respectively, cooperatively stimulating BMP and Wnt signals to induce osteogenesis. Independent of Trb3/Smad4 regulation, Trb3 interacted with β-catenin and activated Wnt signaling to suppress adipogenesis.

3.3 Creation of gene-activated GelCA-PLGA scaffold

Our data displayed that Trb3 is a crucial molecular switch that directs the shift of adipocyte to osteoblast differentiation, indicating that Trb3 is a potential therapeutic target for bone regeneration. Adeno-associated virus (AAV), with excellent safety performance and low immune response, serves as a desirable gene delivery vehicle for molecular therapy (41,42). Further development of biomaterial-based AAV-mediated local gene delivery represents a broader impact on translational application. Here we developed a gelatin-conjugated caffeic acid coated Apatite/PLGA scaffold (GelCA-PLGA) with the incorporation of AAV2-encoding full-length Trb3 (AAV-Trb3) (Fig. 4a and Fig. S3). The chemical conjugation of caffeic acid to gelatin was confirmed by ^{1}H NMR (Fig. 4b). The FTIR spectra of PLGA scaffolds showed a peak at 1769 cm^{-1}, corresponding to COO^{-} of PLGA (Fig. 4c). Ap-PLGA scaffolds exhibited peaks for PO_4^{-3} at 1032, 602, and 561 cm^{-1}. Amide I and II of GelCA were appeared at 1661 and 1552 cm^{-1}, respectively. SEM images exhibited the typical plate-like structure of apatite coating in Ap-PLGA scaffolds. GelCA coating did not significantly alter the porous morphology of the scaffold but the pore wall surface became smoother after the coating in particular with 1% GelCA (Fig 4d). EDX analysis confirmed apatite formation on the surface of PLGA scaffolds as shown by the appearance of calcium (Ca) and phosphorous (P) peaks (Fig. 4e, Table S3). The GelCA scaffolds showed a nitrogen (N) peak, indicating the presence of GelCA coating. These results indicate that GelCA was successfully coated on the surface of Ap-PLGA scaffolds. Additionally, the coating of GelCA did not significantly affect the mechanical properties of scaffolds (Fig. 4f).

Furthermore, GelCA-coated scaffolds displayed high biocompatibility and supported cell proliferation as detected by Live/Dead and AlamarBlue assay (Fig. S4). The release kinetic analysis showcased that 0.2% or 1% GelCA-coated scaffolds released AAV particles in a highly sustained manner up to day 14 in the absence or presence of collagenase, with approximately 8% of initial release, while non-GelCA-coated scaffolds had a burst manner with approximately 32% of initial release (Fig. S5). FACS analysis also illustrated that 0.2% GelCA-coated scaffolds exhibited higher transfection efficiency (~74%) than 1% GelCA-coated scaffold (~68%) or non-GelCA-coated scaffold (~19%) (Fig. 5a). According to these outcomes, we further investigated the interaction of AAV, cell and GelCA on the scaffold (Fig. 5b). Both EGFP-expressed AAV particles and mMSCs were loaded into scaffolds with

pheophorbide A-conjugated GelCA for 72 hours and directly monitored using a confocal laser scanning microscopy. Fluorescence of cells that internalized both EGFP and pheophorbide A was significantly increased in 0.2% GelCA-coated scaffold, revealing the correlation of GelCA and AAV transduction efficiency with seeded cell on the surface of scaffold (Fig. 5b). In addition, GelCA elevated to 1% showed the reduced GFP internalization (Fig. 5b). Together, these outcomes indicated that AAV transfection efficiency was dose-dependently related to GelCA in scaffold. Lastly, we examined how gene-activated GelCA-coated scaffold affects the differentiation of MSCs. GelCA (0.2%)-coated scaffolds loaded with AAV-Trb3 exhibited the increased osteogenic differentiation of mMSCs as shown with elevated ALP activities measured by ALP stain/quantification (Fig. 5c,d). The incorporation of AAV-Trb3 particles with higher titer mediated the higher expression level of ALP. Moreover, the expression of osteogenic genes such as *Runx2, osterix*, and *OCN* was greatly increased with AAV-Trb3 (Fig. 5e). The expression levels of ALP and osteogenic genes mediated by AAV-Trb3 in GelCA scaffolds were significantly higher than Ap-PLGA scaffolds loaded with AAV-Trb3 via physical adsorption without GelCA (Fig. 5e).

3.4 Local delivery of Trb3 promotes mandibular bone regeneration *in vivo*

Large segmental mandibular defects are usually caused by trauma, tumor resection or degenerative diseases, representing an exclusive medical challenge to surgical reconstruction (43). To translate Trb3-mediated osteogenic commitment into a clinically related large mandibular defect model, local surgical delivery of Trb3 (0.2% GelCA-modified scaffold with the incorporation of AAV-Trb3) was conducted in a critical-sized (5×5 mm) mandibular defect created in wild-type rat (Fig. 6a). Twelve weeks post-operation, high-resolution micro-CT images revealed that delivery of AAV-Trb3 at 2.5×10^{11} GC (low dose) and 2.5×10^{12} GC (high dose) induced significant bone formation in mandibular defects (Fig. 6b). Notably, the defects treated with high dose AAV-Trb3 resulted in almost complete bone healing comparable to native mandibular bone (Fig. 6b).

New bone formation visualized by micro-CT images was further confirmed through histological evaluation. H&E stains showcased that large mature bone as well as osteoid matrix was distributed in area of mandibular defects as treated with high dose AAV-Trb3 (Fig. S6a). Conversely, inadequate ossification was detected in the defects treated with scaffold alone or low dose AAV-Trb3 (Fig. S6a). Quantitative analysis displayed that defects treated with high dose AAV-Trb3 increased bone healing, amounting to ~90% and ~60% by new bone areas and BV/TV, respectively (Fig. 6c,d). Analysis of TN and BMD also revealed a significant increase in defects treated with high dose AAV-Trb3 as compared to lose dose AAV-Trb3 or scaffold alone (Fig. 6e,f). Moreover, Masson trichrome stain displayed that a large amount of new bone was detected throughout the defects treated with high dose AAV-Trb3 (Fig. 6g). To assess the quality of bone healing, Picrosirius red stain was applied to detect the organization and distribution of collagen in the area of mandibular defects using polarized light microscopy (Fig. 6g). The high density and mixed birefringence of collagen matrixes was visualized in the defects treated with high dose AAV-Trb3, further proving the regenerated osseous tissues comparable to native bone. As shown by IHC stain, higher level of OCN was also detected in the defects treated with high dose AAV-Trb3 compared to with

low dose AAV-Trb3 or control (Fig. 6g). These results demonstrated that delivery of Trb3 exerted robust osteogenic commitment *in vivo* and significantly promoted bone regeneration even in large osseous defect environment. To further investigate whether Trb3 stimulates osteogenic commitment via BMP and Wnt signals *in vivo* (Fig. S6b,c), the implant at day 14 was collected postoperatively and analyzed by immunofluorescence stain and quantification. Defects treated with AAV-Trb3 at doses of 2.5×10^{12} GC exhibited the remarkably increased expression of Trb3, pSmad1/5/8 and Lef1 as compared to scaffold alone, validating Trb3-mediated in-vivo osteogenic commitment through activating BMP and Wnt signals (Fig. 6h–m).

3.5 *In vivo* local delivery of Trb3 enhances bone regeneration and inhibits fat-filled cyst formation

BMP2, a FDA-approved osteoinductive factor, is widely accepted in the treatment of various bone fractures and defects (44,45). However, the clinical requirement of supraphysiological milligram doses may be associated with inappropriate adipogenesis that further results in abnormal fatty marrow and cyst-like hollow bone, which significantly decreases the quality of BMP2-mediated bone therapy (46). Here we investigated whether delivery of Trb3 could improve osseous regeneration in a clinically related mandibular defect model treated with high dose BMP2. Besides delivering AAV particles, 0.2% GelCA-coated Ap-PLGA scaffold was adopted to deliver BMP2 (Fig. 4a). Release kinetic analysis showed that such GelCA-coated scaffolds released BMP2 with a sustained fashion in the absence or presence of collagenase, and both non-GelCA and GelCA-coated scaffolds had no significant difference (Fig. S7). Furthermore, 30μg BMP2 loaded onto GelCA-PLGA scaffold, which was implanted into rat critical-sized (5×5mm) mandibular bone defects, was detected to induce apparent fat-filled cyst formation in defect area (associated with clinical BMP2-based bone defect treatment) after 12 weeks postoperatively, as detected by micro-CT and histological/immunohistochemical analysis (Fig. 7a,b). Co-delivery of BMP2 (30μg) and AAV-Trb3 (2.5×10^{12} GC) displayed significant improvement of bone healing without obvious cyst formation as examined by micro-CT and sagittal analysis (Fig. 7a,b). Quantitative analysis further revealed that such combinatorial treatment exhibited a significant increase in BV/TV, TN and DBM, and reverted irregular bone healing to the regular one as shown with normal new bone area and bone thickness (Fig. 7c–g).

Moreover, histological evaluation confirmed that such combinatorial treatment exerted a large amount of condensed trabecular bone in mandibular defect area (Fig. 7b). IHC stain/quantification of OCN and Runx2 displayed that defects treated with high dose AAV-Trb3 and BMP2 appeared in a large number of osteoblast-like cells while high dose BMP2 alone showed few osteoblast-like cells (Fig. 7h–j). In contrast, there are fewer adipocyte-like cells observed in area of defects treated with high dose AAV-Trb3 and BMP2 than with BMP2 alone, as detected by IHC stain of PPARγ and OR stain (Fig. 7k–m). Collectively, *in vivo* local delivery of Trb3 using a GelCA-PLGA scaffold improved BMP2-mediated osseous defect repair while simultaneously suppressing fat formation (Fig. 7n).

4. Discussion

Our data has displayed that Trb3 stimulated osteoblastic differentiation while suppressing adipogenic differentiation, indicating that Trb3 is a crucial molecular switch determining MSC lineage commitment. Mechanistically, Trb3 exerted its pro-osteogenic and anti-adipogenic effect through cooperatively activating BMP/Smad and Wnt/β-catenin signals. In a proof-of-principle study, Trb3 induced significant bone formation similar to our previous findings with phenamil, a small molecule BMP stimulator, in a critical sized calvarial defect model (22,29). To demonstrate Trb3 efficacy in inducing bone repair in large defects and minimizing potential adverse effects of current osteoinductive therapeutics, we used a mandibular defect model already established for abnormal bone associated with high BMP doses (47). *In vivo* delivery of Trb3 further demonstrated robust bone formation and apparent fat inhibition in the treatment of mandibular bone defects. These findings support that Trb3 is an important therapeutic target for tissue regeneration and bone-related diseases.

Identifying molecular switch of MSC fate commitment is extraordinarily useful for creation of efficacious bone therapeutic approach (14). Although different transcriptional factors or signaling pathways have been found in regulating osteoblast and adipocyte differentiation, the molecular switch specifically governing MSC fate remains poorly understood (9,10). Trb3 was identified as a key molecular switch for modulating adipo-osteogenic balance, which may fill an important knowledge gap and facilitate bone therapeutics. BMP2-based treatment is a representative and common therapeutic approach for clinical bone defect repair (48). Nonetheless, increasing experimental and clinical evidences suggest that the therapeutic effect of high-dose BMP2 may be compromised with increased adipogenesis and reduced osteogenic commitment (44–46). We previously demonstrated undesired cyst-like bone formation induced by BMP2 treatment at high dose over 600 μg/ml (30 μg per defect) in a rat mandibular defect model (47). Although BMP2 has species-specific dose requirements (1.5 mg/ml for human use), adverse effects of BMP2 are dose-related, and thus we delineated the role of Trb3 in improving BMP2-induced bone formation quality in the rat model. Our *in vivo* observation displayed that Trb3 significantly enhanced BMP2-mediated bone regeneration while simultaneously suppressing marrow adiposity in a clinically related mandibular defect model (Fig. 7), further highlighting that molecular modulation of adipo-osteogenic balance is a promising therapeutic strategy for tissue-engineered bone repair.

Imbalance of adipo-osteogenic differentiation is associated not only with tissue-engineered bone repair but also with some pathological bone loss related diseases. Of note, age-related osteoporosis is a substantial health problem, characterized by imbalance of metabolism and bone remodeling due to elevated marrow fat and low bone mass (6–7). Currently, bisphosphonates are the frontline antiresorptive pharmacotherapy for osteoporosis (49). However, severe complications are increasingly observed in clinical treatment due to their excessive suppression of bone turnover (49). Thus, modulating adipo-osteogenic balance via Trb3 might also be an effective anabolic alternative potentially used for treatment of osteoporotic-related bone loss diseases.

Recent studies have reported that Trb3 affects development and cellular differentiation through interaction with various transcriptional factors (15,17,25). However, the molecular

mechanisms by which Trb3 regulates MSC fate commitment are not clear. Both BMP/Smad and Wnt/β-catenin signals have been demonstrated to exert crucial roles in adipogenic and osteogenic differentiation (50). As expected, our mechanistic analysis revealed that Trb3 controlled MSC lineage commitment through BMP and Wnt signals (Fig. 3). Moreover, we found that Trb3 bound to Smad4 and β-catenin respectively and in turn activated BMP and Wnt pathways respectively, synergistically promoting osteoblastic differentiation (Fig. 3). We also found that Trb3 bound to β-catenin and activated Wnt signaling only to suppress adipogenic differentiation (Fig. 3). Several studies have illustrated crosstalk between BMP and Wnt signal on cell fate determination (51,52). For example, previous studies demonstrated that Smad4 in murine embryonic stem cells was involved in Lef1 transcriptional complex in response to β-catenin activation (53). In our studies, Trb3 was revealed to bind to Smad4 and β-catenin separately (Fig. 3). It is interesting to elucidate whether Trb3, Smad4 and β-catenin forms a complex to regulate MSC differentiation in future study. In addition, although the current findings of Trb3 and its molecular mechanisms on MSC lineage commitment were conducted by comprehensive molecular and genetic approaches, the additional role of Trb3 on MSC function and differentiation may be further exploited in transgenic or knockout mice *in vivo* in future.

In our work, the GelCA-PLGA scaffold was created to deliver AAV-Trb3 for in-vivo bone regeneration (Fig. 4). PLGA scaffold with biomimetic apatite coating not just exerted the enhanced osteoconductivity but also acted as a suitable carrier for small molecule and protein delivery (54). However, Apatite/PLGA scaffold applied to AAV delivery revealed a highly burst manner and low transfection efficiency (Fig. 5 and Fig. S5). Thus, the further modification of Apatite/PLGA scaffold that is capable of delivering AAV particles may facilitate the translational application of gene-based skeletal therapy. Caffeic acid is derived from the extract of propolis produced by honeybees and is increasingly employed in the fields of biomaterials and bone tissue engineering (55, 56). The catechol group contained in caffeic acid can act as a conjugate to vector particles (such as AAV) or growth factors (such as BMP2) containing amines and/or thiols via Schiff base reaction and Michael type addition (57–59). Gelatin - a native protein obtained from collagen hydrolysis possesses multiple appropriate sites for cellular adhesion, which is commonly applied for improvement of cell-material interaction (60,61). Taken together, gelatin-conjugated caffeic acid immobilized with AAV particles was coated onto the surface of Apatite/PLGA backbone, which was anticipated to reduce AAV burst release and increase its transduction efficiency. Indeed, the experimental outcomes indicated that the GelCA-coated hybrid scaffold released AAV particles in a sustained manner and elevated the transduction efficiency of AAV in the seeded MSCs (Fig. 5 and Fig. S5). Overall, the creation of GelCA-based hybrid scaffold offers an effective means to locally deliver genes, potentially broadening the translational use of Trb3-mediated tissue regeneration.

5. Conclusions

In this study, we found Trb3 serves as a key molecular switch controlling adipocyte-osteoblast differentiation in MSCs. We also found that Trb3 regulates MSC lineage fate through stimulating BMP and Wnt signaling. Furthermore, we employed scaffold-mediated local Trb3 transfer to demonstrate a practical approach for improved bone healing in a

clinically-related mandibular bone defect model. Our findings not just provide new molecular insights on MSC lineage fate but also pose a promising therapeutic approach for clinical skeletal regeneration and related disease treatment.

Supplementary Material

Refer to Web version on PubMed Central for supplementary material.

Acknowledgements

This work was supported by grants from the National Institutes of Health (R01 DE027332), the Department of Defense (W81XWH-18-1-0337), and MTF Biologics. We thank UCLA Translational Pathology Core Laboratory (TPCL) for making tissue section, The Technology Center for Genomics & Bioinformatics (TCGB) for conducting RNA-seq, and The Janis V. Giorgi Flow Cytometry Core Facility for performing FACS analysis. We thank Ms. Olga Bezouglaia for care of animal and animal surgery.

References

1. Einhorn TA, Gerstenfeld LC, Fracture healing: mechanisms and interventions. Nat Rev Rheumatol. 11, 45–54 (2015). [PubMed: 25266456]
2. Cowan CM, Shi YY, Aalami OO, Chou YF, Mari C, Thomas R, Quarto N, Contag CH, Wu B, Longaker MT, Adipose-derived adult stromal cells heal critical-size mouse calvarial defects. Nat Biotechnol. 22, 560–567 (2004). [PubMed: 15077117]
3. Rachner TD, Khosla S, Hofbauer LC, Osteoporosis: now and the future. Lancet. 9, 377, 1276–87 (2011).
4. Pittenger MF, Mackay AM, Beck SC, Jaiswal RK, Douglas R, Mosca JD, Moorman MA, Simonetti DW, Craig S, Marshak DR, Multilineage potential of adult human mesenchymal stem cells. Science. 284, 143–147 (1999). [PubMed: 10102814]
5. Zhou BO, Yue R, Murphy MM, Peyer JG, Morrison SJ, Leptin-receptor-expressing mesenchymal stromal cells represent the main source of bone formed by adult bone marrow. Cell Stem Cell. 15, 154–168 (2014) [PubMed: 24953181]
6. Pei L, Tontonoz P Fat's loss is bone's gain. J Clin Invest. 113, 805–806 (2004). [PubMed: 15067310]
7. Horwitz EM, Prockop DJ, Fitzpatrick LA, Koo WW, Gordon PL, Neel M, Sussman M, Orchard P, Marx JC, Pyeritz RE, Brenner MK, Transplantability and therapeutic effects of bone marrow-derived mesenchymal cells in children with osteogenesis imperfecta. Nat Med. 5, 309–313 (1999). [PubMed: 10086387]
8. Picke AK, Campbell GM, Blüher M, Krügel U, Schmidt FN, Tsourdi E, Winzer M, Rauner M, Vukicevic V, Busse B, Salbach-Hirsch J, Tuckermann JP, Simon JC, Anderegg U, Hofbauer LC, Saalbach A, Thy-1 (CD90) promotes bone formation and protects against obesity. Sci Transl Med. 10 (2018).
9. Huang W, Yang S, Shao J, Li YP, Signaling and transcriptional regulation in osteoblast commitment and differentiation. Front Biosci. 12, 3068–3092 (2007). [PubMed: 17485283]
10. Kawai M, Rosen CJ, PPARgamma: a circadian transcription factor in adipogenesis and osteogenesis. Nat Rev Endocrinol. 6, 629–636 (2010). [PubMed: 20820194]
11. Li J, Liu X, Zuo B, Zhang L, The Role of Bone Marrow Microenvironment in Governing the Balance between Osteoblastogenesis and Adipogenesis. Aging Dis. 7, 514–525 (2015). [PubMed: 27493836]
12. Rogers MB, Shah TA, Shaikh NN, Turning Bone Morphogenetic Protein 2 (BMP2) on and off in Mesenchymal Cells. J Cell Biochem. 116, 2127–2138 (2015). [PubMed: 25776852]
13. Ross SE, Hemati N, Longo KA, Bennett CN, Lucas PC, Erickson RL, MacDougald OA, Inhibition of adipogenesis by Wnt signaling. Science. 289, 950–953 (2000). [PubMed: 10937998]

14. Takada I, Kouzmenko AP, Kato S, Molecular switching of osteoblastogenesis versus adipogenesis: implications for targeted therapies. Expert Opin Ther Targets. 13, 593–603 (2009). [PubMed: 19397478]
15. Qi L, Heredia JE, Altarejos JY, Screaton R, Goebel N, Niessen S, Macleod IX, Liew CW, Kulkarni RN, Bain J, Newgard C, Nelson M, Evans RM, Yates J, Montminy M, TRB3 links the E3 ubiquitin ligase COP1 to lipid metabolism. Science. 312, 1763–1766 (2006). [PubMed: 16794074]
16. Avery J, Etzion S, DeBosch BJ, Jin X, Lupu TS, Beitinjaneh B, Grand J, Kovacs A, Sambandam N, Muslin AJ, TRB3 function in cardiac endoplasmic reticulum stress. Circ Res. 106, 1516–1523 (2010). [PubMed: 20360254]
17. Ohoka N, Yoshii S, Hattori T, Onozaki K, Hayashi H, TRB3, a novel ER stress-inducible gene, is induced via ATF4-CHOP pathway and is involved in cell death. EMBO J. 24, 1243–1255 (2005). [PubMed: 15775988]
18. Du K, Herzig S, Kulkarni RN, Montminy M, TRB3: a tribbles homolog that inhibits Akt/PKB activation by insulin in liver. Science 300,1574–1577 (2003). [PubMed: 12791994]
19. Staines KA, Zhu D, Farquharson C, MacRae VE, Identification of novel regulators of osteoblast matrix mineralization by time series transcriptional profiling. J Bone Miner Metab. 32, 240–251 (2014). [PubMed: 23925391]
20. Chan MC, Nguyen PH, Davis BN, Ohoka N, Hayashi H, Du K, Lagna G, Hata A, A novel regulatory mechanism of the bone morphogenetic protein (BMP) signaling pathway involving the carboxyl-terminal tail domain of BMP type II receptor. Mol. Cell. Biol. 27, 5776–5789 (2007). [PubMed: 17576816]
21. Fan J, Guo M, Im CS, Pi-Anfruns J, Cui ZK, Kim S, Wu BM, Aghaloo TL, Lee M, Enhanced Mandibular Bone Repair by Combined Treatment of Bone Morphogenetic Protein 2 and Small-Molecule Phenamil. Tissue Eng Part A. 23, 195–207 (2017). [PubMed: 27771997]
22. Fan J, Pi-Anfruns J, Im CS, Guo M, Cui ZK, Fartash A, Kim S, Patel N, Bezouglaia O, Wu BM, Wang CY, Aghaloo TL, Lee M, Enhanced Osteogenesis of Adipose-Derived Stem Cells by Regulating Bone Morphogenetic Protein Signaling Antagonists and Agonists. Stem Cells Transl Med. 5, 539–551 (2016). [PubMed: 26956209]
23. Takahashi Y, Ohoka N, Hayashi H, Sato R, TRB3 suppresses adipocyte differentiation by negatively regulating PPARgamma transcriptional activity. J Lipid Res. 49, 880–892 (2008). [PubMed: 18187772]
24. Kim YD, Pofali P, Park TE, Singh B, Cho K, Maharjan S, Dandekar P, Jain R, Choi YJ, Arote R, Cho CS, Gene therapy for bone tissue engineering. Tissue Eng. Regen. Med. 13, 111–125 (2016). [PubMed: 30603391]
25. Gower RM, Shea LD, Biomaterial Scaffolds for Controlled, Localized Gene Delivery of Regenerative Factors. Adv Wound Care (New Rochelle). 2,100–106 (2013). [PubMed: 24527333]
26. Chen R, Zhang H, Yan J, Bryers J, Scaffold-mediated delivery for non-viral mRNA vaccines. Gene Ther. 25, 556–567 (2018). [PubMed: 30242259]
27. Gu DL, Nguyen T, Gonzalez AM, Printz MA, Pierce GF, Sosnowski BA, Phillips ML, Chandler LA, Adenovirus encoding human platelet-derived growth factor-B delivered in collagen exhibits safety, biodistribution, and immunogenicity profiles favorable for clinical use. Mol Ther. 9, 699–711 (2004). [PubMed: 15120331]
28. Keeney M, Chung MT, Zielins ER, Paik KJ, McArdle A, Morrison SD, Ransom RC, Barbhaiya N, Atashroo D, Jacobson G, Zare RN, Longaker MT, Wan DC, Yang F, Scaffold-mediated BMP-2 minicircle DNA delivery accelerated bone repair in a mouse critical-size calvarial defect model. J. Biomed. Mater. Res., Part A. 104, 2099–2107 (2016).
29. Fan J, Im CS, Cui ZK, Guo M, Bezouglaia O, Fartash A, Lee JY, Nguyen J, Wu BM, Aghaloo T, Lee M, Delivery of Phenamil Enhances BMP-2-Induced Osteogenic Differentiation of Adipose-Derived Stem Cells and Bone Formation in Calvarial Defects. Tissue Eng Part A. 21, 2053–65 (2015). [PubMed: 25869476]
30. Lee S, Shen J, Pan HC, Shrestha S, Asatrian G, Nguyen A, Meyers C, Nguyen V, Lee M, Soo C, Ting K, James AW, Calvarial Defect Healing by Small Molecule Smoothened Agonist, Tissue Eng Part A. 22,1357–1366 (2016). [PubMed: 27702396]

31. Shen J, James AW, Zhang X, Pang S, Zara JN, Asatrian G, Chiang M, Lee M, Khadarian K, Nguyen A, Lee KS, Siu RK, Tetradis S, Ting K, Soo C, Novel Wnt Regulator NEL-Like Molecule-1 Antagonizes Adipogenesis and Augments Osteogenesis Induced by Bone Morphogenetic Protein 2. Am J Pathol. 186, 419–34 (2016). [PubMed: 26772960]
32. Levi B, Nelson ER, Li S, James AW, Hyun JS, Montoro DT, Lee M, Glotzbach JP, Commons GW, Longaker MT, Dura mater stimulates human adipose-derived stromal cells to undergo bone formation in mouse calvarial defects. Stem Cells. 29,1241–55 (2011). [PubMed: 21656608]
33. Lee CS, Kim S, Fan J, Hwang HS, Aghaloo T, Lee M, Smoothened agonist sterosome immobilized hybrid scaffold for bone regeneration. Sci. Adv. 6, eaaz7822 (2020). [PubMed: 32494652]
34. Lee H, Dellatore SM, Miller WM, Messersmith PB, Mussel-inspired surface chemistry for multifunctional coatings. Science 318, 426–430 (2007). [PubMed: 17947576]
35. Sedo J, Saiz-Poseu J, Busque F, Ruiz-Molina D, Catechol-based biomimetic functional materials. Adv. Mater. 25, 653–701 (2013). [PubMed: 23180685]
36. Iacomino M, Paez JI, Avolio R, Carpentieri A, Panzella L, Falco G, Pizzo E, Errico ME, Napolitano A, Del Campo A, d'Ischia M, Multifunctional Thin Films and Coatings from Caffeic Acid and a Cross-Linking Diamine. Langmuir. 33, 2096–2102 (2017). [PubMed: 28191981]
37. Gómez-Guillén MC, Giménez B, López-Caballero ME, Montero MP, Functional and bioactive properties of collagen and gelatin from alternative sources: A review. Food Hydrocolloids. 25, 1813–182 (2011).
38. Wang J, Li D, Li T, Ding J, Liu J, Li B, Chen X, Gelatin Tight-Coated Poly(lactide-co-glycolide) Scaffold Incorporating rhBMP-2 for Bone Tissue Engineering. Materials (Basel). 8,1009–1026 (2015). [PubMed: 28787985]
39. Raucci MG, D'Amora U, Ronca Alfredo., Demitri C, Ambrosio L, Bioactivation Routes of Gelatin Based Scaffolds to Enhance at Nanoscale Level Bone Tissue Regeneration. Front Bioeng Biotechnol. 7,27(2019) [PubMed: 30828576]
40. Bello AB, Kim D, Kim D, Park H, Lee S, Engineering and Functionalization of Gelatin Biomaterials: From Cell Culture to Medical Applications. Tissue Engineering Part B: Reviews. 26,164–180 (2020). [PubMed: 31910095]
41. Asokan A, Conway JC, Phillips JL, Li C, Hegge J, Sinnott R, Yadav S, DiPrimio N, Nam HJ, Agbandje-McKenna M, McPhee S, Wolff J, Samulski RJ, Reengineering a receptor footprint of adeno-associated virus enables selective and systemic gene transfer to muscle. Nat Biotechnol. 28, 79–82 (2010). [PubMed: 20037580]
42. Evans CH, Gene delivery to bone. Adv Drug Deliv Rev 64, 1331–1340 (2012). [PubMed: 22480730]
43. Hadloc TA, Vacanti JP, Cheney ML, Tissue engineering in facial plastic and reconstructive surgery. Facial Plast Surg. 14, 197 (1998) [PubMed: 11816192]
44. James AW, LaChaud G, Shen J, Asatrian G, Nguyen V, Zhang X, Ting K, Soo C A Review of the Clinical Side Effects of Bone Morphogenetic Protein-2. Tissue Eng Part B Rev. 22, 284–297 (2016). [PubMed: 26857241]
45. Smucker JD, Rhee JM, Singh K, Yoon ST, Heller JG, Increased swelling complications associated with off-label usage of rhBMP-2 in the anterior cervical spine. Spine (Phila Pa 1976). 31, 2813–2819 (2006). [PubMed: 17108835]
46. Zara JN, Siu RK, Zhang X, Shen J, Ngo R, Lee M, Li W, Chiang M, Chung J, Kwak J, Wu BM, Ting K, Soo C, High doses of bone morphogenetic protein 2 induce structurally abnormal bone and inflammation in vivo. Tissue Eng Part A. 17, 1389–1399 (2011). [PubMed: 21247344]
47. Fan J, Pi-Anfruns J, Guo M, Im DCS, Cui ZK, Kim S, Wu BM, Aghaloo TL, Lee M, Small molecule-mediated tribbles homolog 3 promotes bone formation induced by bone morphogenetic protein-2. Sci. Rep. 7, 7518 (2017). [PubMed: 28790361]
48. Johnson CT, Sok MCP, Martin KE, Kalelkar PP, Caplin JD, Botchwey EA, García AJ, Lysostaphin and BMP-2 co-delivery reduces S. aureus infection and regenerates critical-sized segmental bone defects. Sci Adv. 5, eaaw1228 (2019). [PubMed: 31114804]
49. Black DM, Rosen CJ, Clinical Practice. Postmenopausal Osteoporosis. N Engl J Med. 374, 254–62 (2016). [PubMed: 26789873]

50. Feng J, Jing J, Li J, Zhao H, Punj V, Zhang T, Xu J, Chai Y, BMP signaling orchestrates a transcriptional network to control the fate of mesenchymal stem cells in mice. Development. 144, 2560–2569 (2017). [PubMed: 28576771]
51. Guo X, Wang XF, Signaling cross-talk between TGF-beta/BMP and other pathways. Cell Res. 19, 71–88 (2009). [PubMed: 19002158]
52. Baik J, Magli A, Tahara N, Swanson SA, Koyano-Nakagawa N, Borges L, Stewart R, Garry DJ, Kawakami Y, Thomson JA, Perlingeiro RC, Endoglin integrates BMP and Wnt signalling to induce haematopoiesis through JDP2. Nat Commun. 7, 13101 (2016). [PubMed: 27713415]
53. Hussein SM, Duff EK, Sirard C, Smad4 and beta-catenin co-activators functionally interact with lymphoid-enhancing factor to regulate graded expression of Msx2. J Biol Chem. 278, 48805–48814 (2003). [PubMed: 14551209]
54. Murphy WL, Kohn DH, Mooney DJ, Growth of continuous bonelike mineral within porous poly(lactide-co-glycolide) scaffolds in vitro. J Biomed Mater Res. 50, 50–58 (2000). [PubMed: 10644963]
55. Kazancioglu HO, Aksakalli S, Ezirganli S, Birlik M, Esrefoglu M, Acar AH, Effect of caffeic acid phenethyl ester on bone formation in the expanded inter-premaxillary suture. Drug Des Devel Ther. 9, 6483–6488 (2015).
56. Jiang RW, Lau KM, Hon PM, Mak TC, Woo KS, Fung KP, Chemistry and biological activities of caffeic acid derivatives from Salvia miltiorrhiza. Curr Med Chem. 12, 237–246 (2005). [PubMed: 15638738]
57. Yang J, Saggiomo V, Velders AH, Cohen Stuart MA, Kamperman M, Reaction Pathways in Catechol/Primary Amine Mixtures: A Window on Crosslinking Chemistry. PLoS One. 11, e0166490 (2016). [PubMed: 27930671]
58. Zhang J, Li J, Jia G, Jiang Y, Liu Q, Yang X, Pan S, Improving osteogenesis of PLGA/HA porous scaffolds based on dual delivery of BMP-2 and IGF-1 via a polydopamine coating. RSC Adv. 7, 56732–56742 (2017).
59. Xu Q, Li Q, Zhu Y, Zhao K, Gu R, Zhu R, Recombinant human BMP-7 grafted poly(lactide-co-glycolide)/hydroxyapatite scaffolds via polydopamine for enhanced calvarial repair. RSC Adv. 8, 27191–27200 (2018).
60. Burmania JA, Stevens KR, Kao WJ, Cell interaction with protein-loaded interpenetrating networks containing modified gelatin and poly(ethylene glycol) diacrylate. Biomaterials. 24, 3921–3930 (2003). [PubMed: 12834587]
61. Cui ZK, Kim S, Baljon JJ, Wu BM, Aghaloo T, Lee M, Microporous methacrylated glycol chitosan-montmorillonite nanocomposite hydrogel for bone tissue engineering. Nat Commun. 10, 3523 (2019). [PubMed: 31388014]

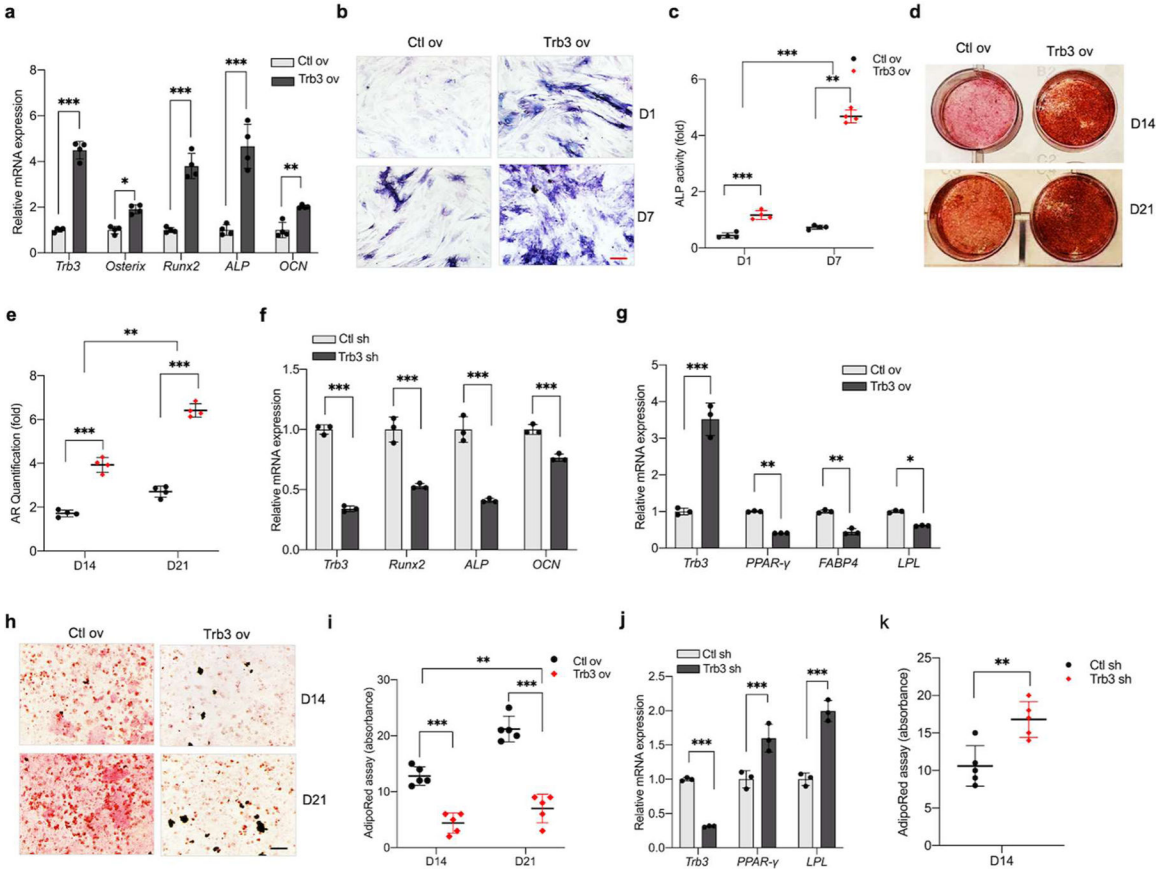

Fig. 1: Trb3 determines the lineage commitment of MSCs.

By genetic approaches, Trb3 was shown to enhance osteogenesis and inhibits adipogenesis *in vitro*. Osteogenic and adipogenic markers were assessed in hMSCs transduced with lentivirus particles encoding full-length Trb3 or Trb3 shRNA. (**a–e**): Trb3 overexpression increased osteogenic gene expression (*Osterix*, *Runx2*, *ALP*, *OCN)* by real-time PCR at day 2 (a), ALP expression by ALP stain/activity at days 1 and 7 (b,c), and mineralization by AR stain/quantification at days 14, 21 (d,e). (**f**): Trb3 knockdown decreased osteogenic gene expression at day 2. (**g–i**): Trb3 overexpression suppressed adipogenic gene expression (*PPAR-γ*, *FABP4*, *LPL*) (g) and lipid accumulation by OR stain (h) and AdipoRed assay (i). (**j,k**): Trb3 knockdown increased adipogenic gene expression (j) and AdipoRed assay (k). Scale bar = 200 μm. hMSCs, human bone marrow mesenchymal stem cells; ALP, alkaline phosphatase; OCN, osteocalcin; AR, alizarin red. OR, Oil red. Values represent mean ± SD: **p* <0.05, ***p* <0.01 and ****p* <0.001 using a two-tailed Student's t-test and one-way ANOVA test.

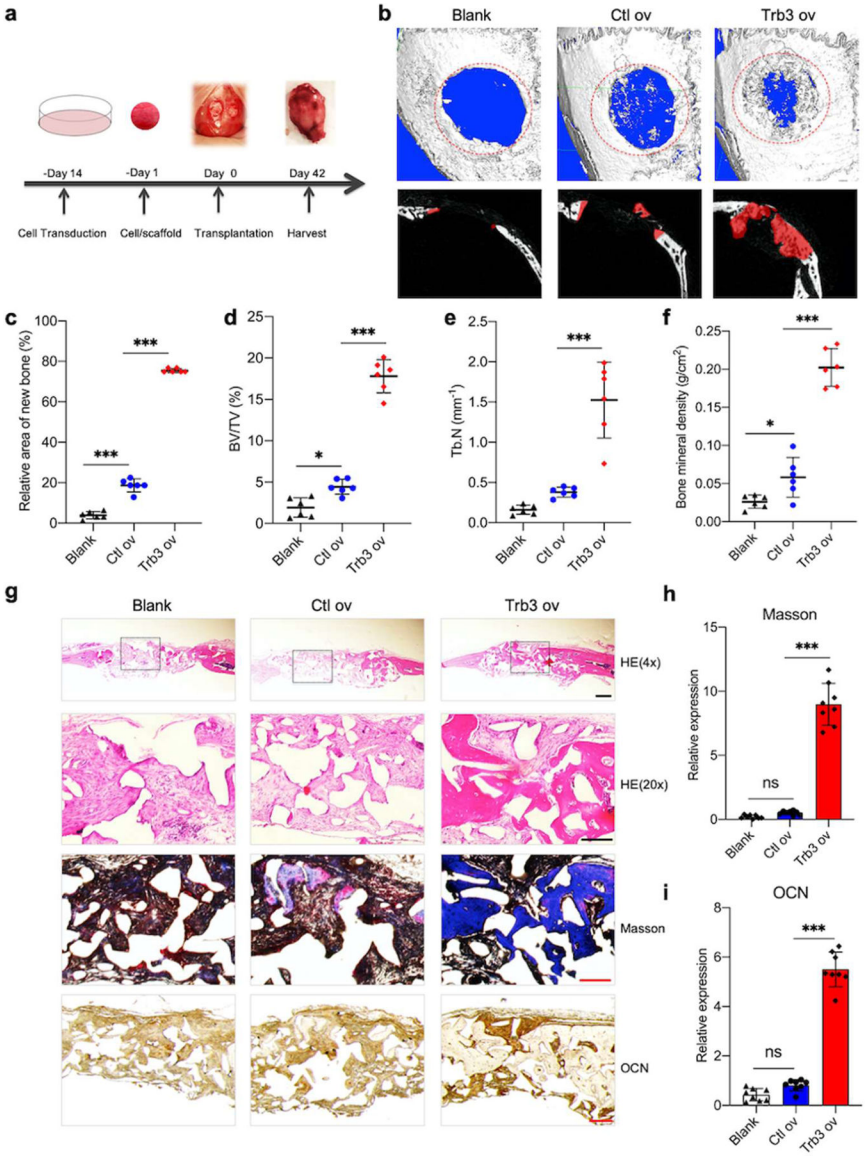

Fig. 2: Trb3 promotes MSC-mediated bone regeneration *in vivo*.

(**a**): hMSCs with Trb3 overexpression or control were seeded onto Apatite/PLGA scaffolds and implanted into critical-sized (3×3mm) calvarial defects created in nude mice (6 mice per group). After 6 weeks postoperatively, the implant was collected for micro-CT and histological analysis. (**b**): micro-CT images of mouse calvarial bone regeneration. New bone formation present in defect area is highlighted with red color. (**c–f**): Quantitative analysis of new bone area, BV/TV, Tb.N and bone mineral density (n=6 per group). (**g**): HE stain, Masson trichrome stain and immunohistochemical stain of OCN. Black box indicates the high magnification of image below. Scale bar = 500 μm (HE at 4x), 200 μm (HE at 20x, Masson, OCN). (**h,i**): Colorimetric quantification of Masson trichrome and OCN stain (n=8 per group). hMSCs, human bone marrow mesenchymal stem cells; BV/TV, bone volume/tissue volume; Tb.N, trabecular number; HE, hematoxylin and eosin. Values represent mean ± SD: ns, not significant, *p <0.05 and ***p <0.001 using one-way ANOVA test.

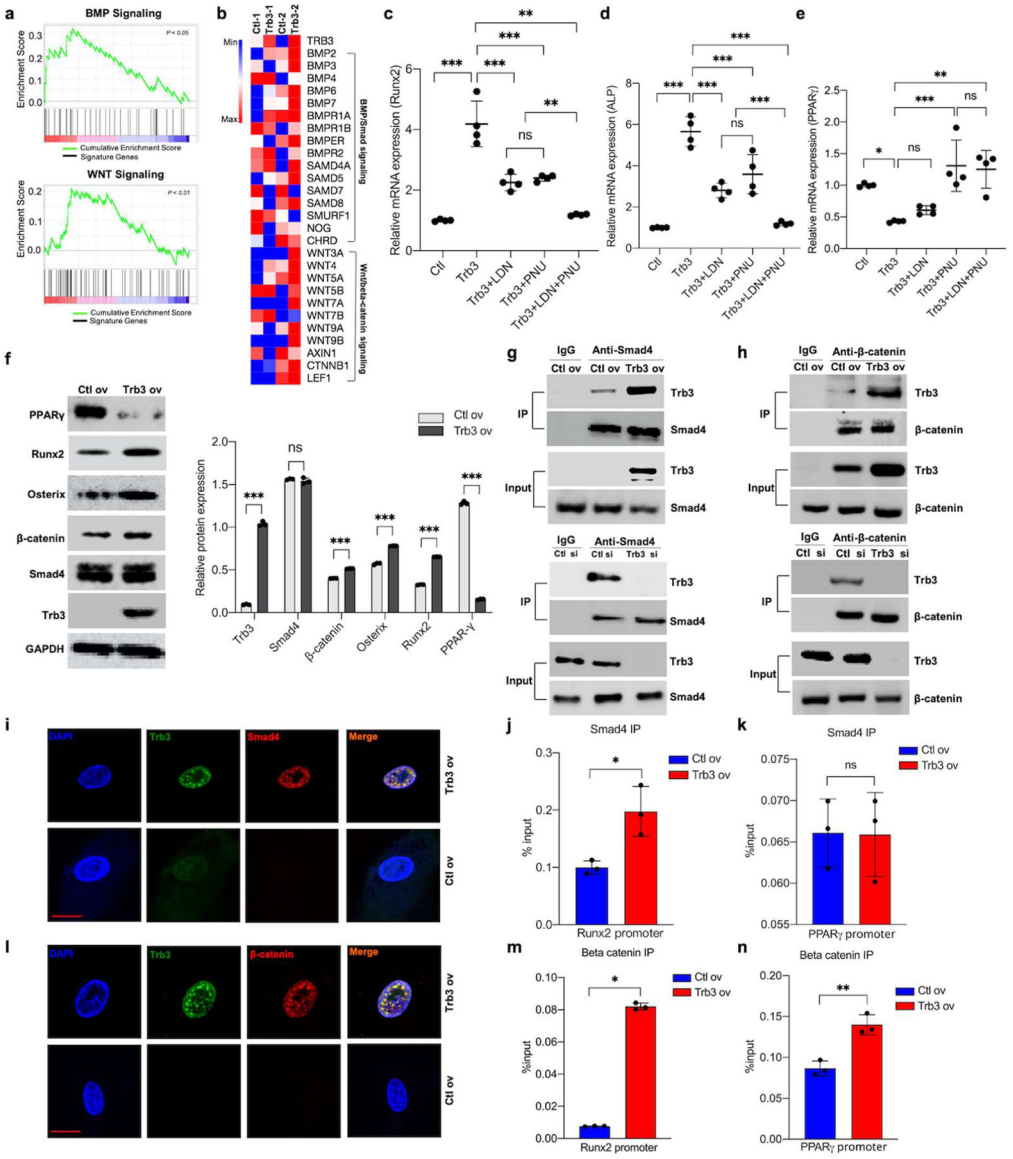

Fig. 3: Trb3 regulates lineage commitment of MSCs by BMP/Smad and Wnt/β-catenin signals.

(**a**): Gene set enrichment analysis (GSEA) of RNA-Seq in hMSCs with and without Trb3 overexpression. (**b**): Heatmap analysis of gene expression related to BMP and Wnt signals. Gene expression profile of hMSCs with Trb3 overexpression and control was conducted by RNA-Seq. Maximum (red) indicates the degree of upregulation and Minimum (blue) indicates downregulation. (**c–e**): Effect of BMP and Wnt inhibitors on MSC lineage commitment. When hMSCs were treated with LDN (BMP inhibitor, 500 nM) or/and PNU (Wnt inhibitor, 10 μM), expression of osteogenic (c,d) and adipogenic (e) genes were respectively measured by real-time PCR assay at day 2. (**f**): Western-blot and quantitative analysis of transcriptional protein expression in hMSCs with Trb3 overexpression and control at 48 hours. (**g,h**): Co-IP of Smad 4 (g) or β-catenin (h) in hMSCs with or without Trb3 overexpression (top) and in hMSCs with or without Trb3 siRNA (below). (**i**): Co-localization of Trb3 with Smad4 in hMSCs was visualized with a confocal microscopy. (**j,k**):

hMSCs with or without Trb3 overexpression underwent ChIP assay using antibodies against Smad4. (**l**): Co-localization of Trb3 with β-catenin was analyzed with a confocal microscopy. (**m,n**): hMSCs with or without Trb3 overexpression underwent ChIP assay using antibodies against β-catenin. Scale bar = 25 μm. hMSCs, human bone marrow mesenchymal stem cells; LDN, LDN193189; PNU, PNU-74654; Co-IP, co-immunoprecipitation; ChIP, chromatin immunoprecipitation. Values represent mean ± SD: ns, not significant, *p < 0.05, ** p <0.01 and *** p <0.001 using a two-tailed Student's t-test and one-way ANOVA test.

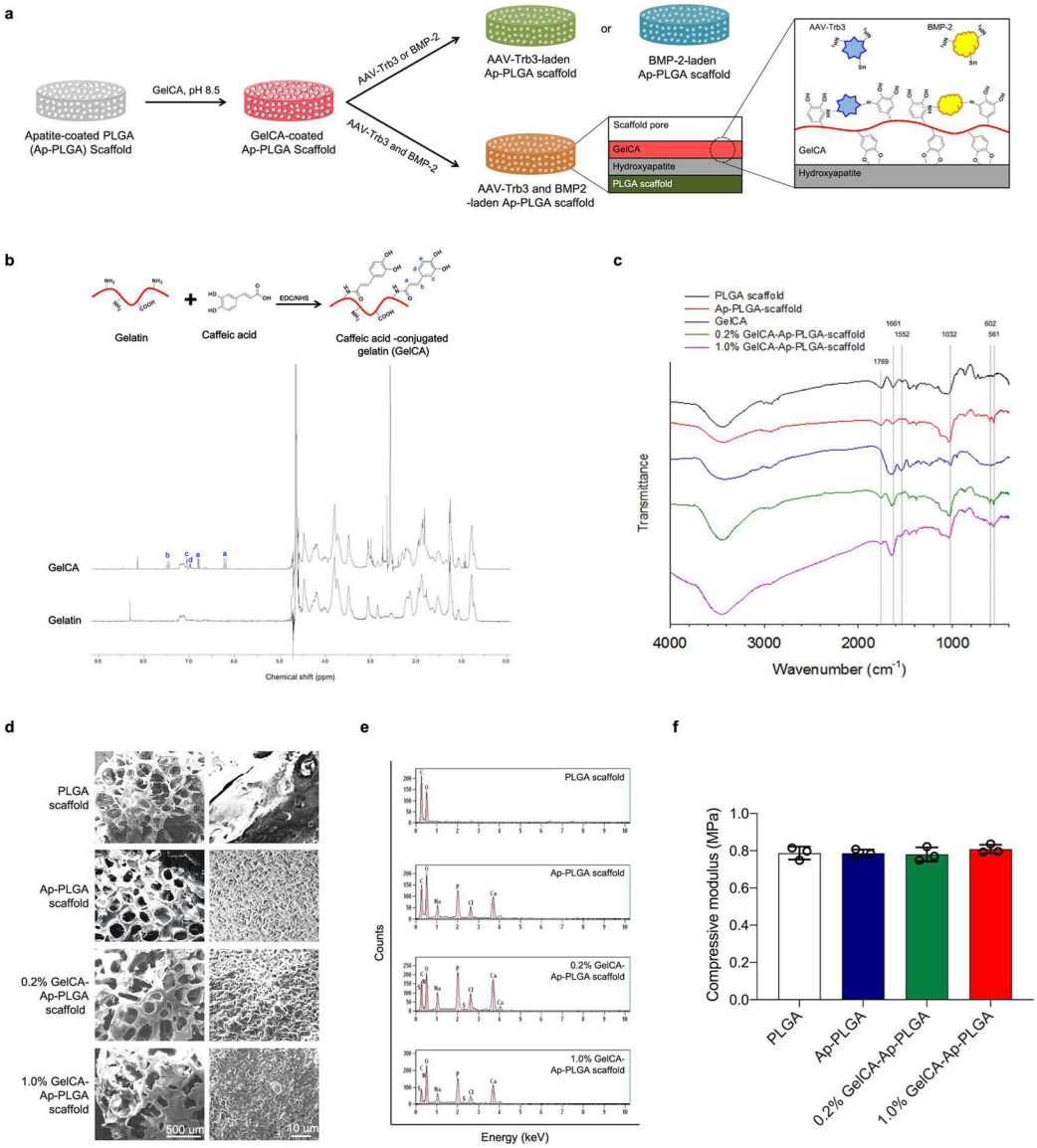

Fig. 4: Characterizations of GelCA-coated Ap-PLGA scaffolds.

(**a**): Schematic diagram of GelCA-PLGA scaffold fabrication through coating gelatin-conjugated caffeic acid onto the surface of Ap-PLGA scaffold. The GelCA-coated hybrid biopolymer scaffold was adopted to deliver AAV2-encoding Trb3 or/and recombinant BMP2 protein. (**b**): ^{1}H NMR spectra of gelatin and caffeic acid-conjugated gelatin (GelCA) in D_2O. (**c**): FTIR spectra of PLGA, Ap-PLGA, 0.2% GelCA-Ap-PLGA, 1.0% GelCA-Ap-PLGA scaffolds, and GelCA. (**d**): SEM images of PLGA, Ap-PLGA, 0.2% GelCA-Ap-PLGA, 1.0% GelCA-Ap-PLGA scaffolds. (**e**): EDX spectra of scaffolds. (**f**): Compressive modulus of scaffolds. Ap-PLGA, apatite-coated PLGA scaffold; SEM, Scanning electron microscope; EDX, Energy-dispersive X-ray spectroscopy; FTIR, Fourier-transform infrared spectroscopy, NMR, Nuclear magnetic resonance spectroscopy.

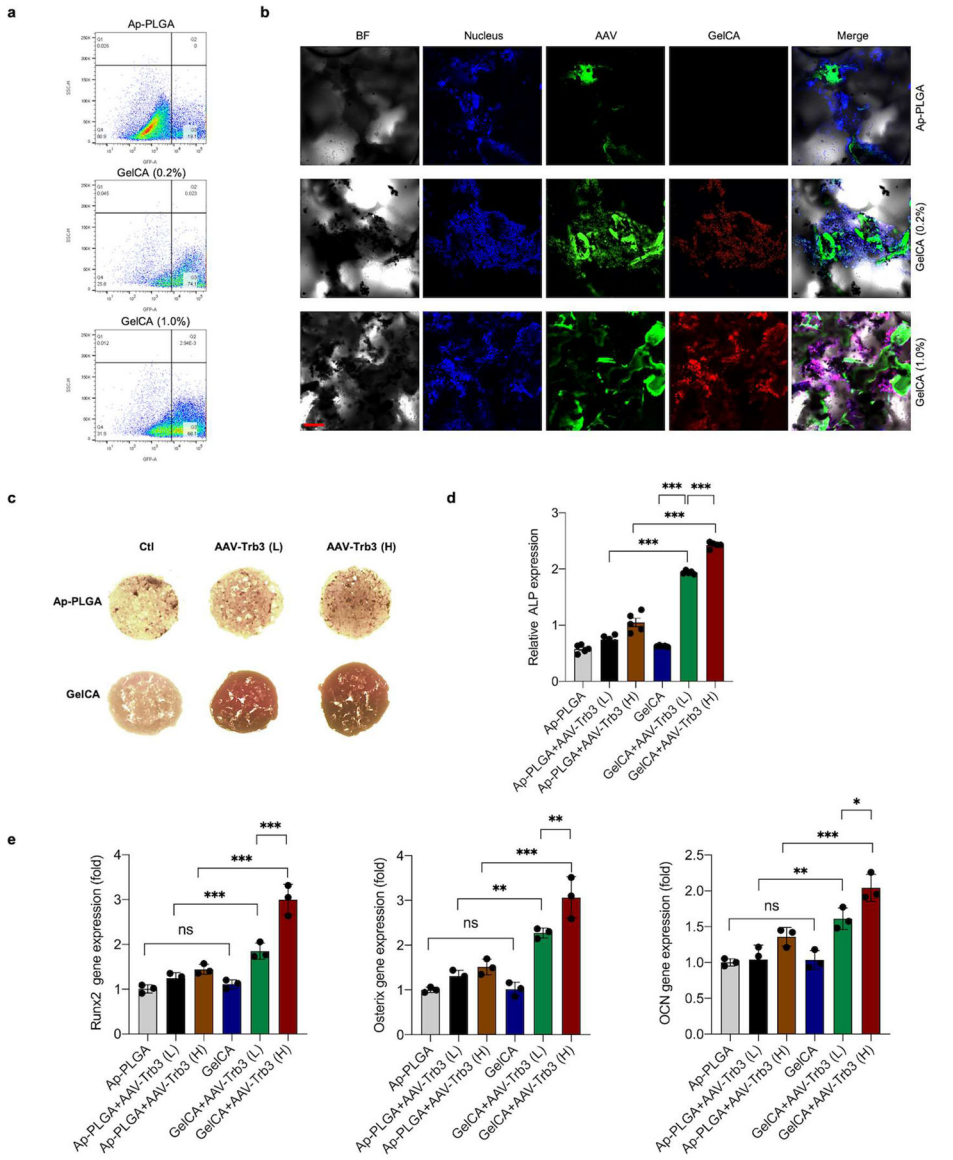

Fig. 5: GelCA-coated Ap-PLGA scaffolds for AAV-Trb3 delivery.

(**a**): FACS analysis of AAV2 transduction efficiency in GelCA-coated scaffold seeded with hMSCs. (**b**): Confocal images of mMSCs with nucleus stain (Hoechst 33343 (blue), GFP-expressed AAV2 particle, pheophorbide A-encapsulated GelCA (red) on the surface of scaffolds. Scale bar = 100 μm. (**c,d**): ALP expression (c) and colorimetric quantification (d) of mMSCs in scaffolds at day 7. (**e**): Expression of osteogenic genes including *Runx2, Osterix,* and *OCN* at day 7 as evaluated by real-time PCR. Ap-PLGA, apatite-coated PLGA scaffold; GelCA, GelCA-coated Ap-PLGA; L, low dose AAV (5×10^{10} GC); H, high dose (5×10^{11} GC); FACS, Fluorescence-activated cell sorting; mMSC, mouse bone marrow mesenchymal stem cells; AAV2, adeno-associated viruses (serotype 2). Values represent mean ± SD: ns, not significant, *p < 0.05, ** p <0.01 and *** p <0.001 using one-way ANOVA test.

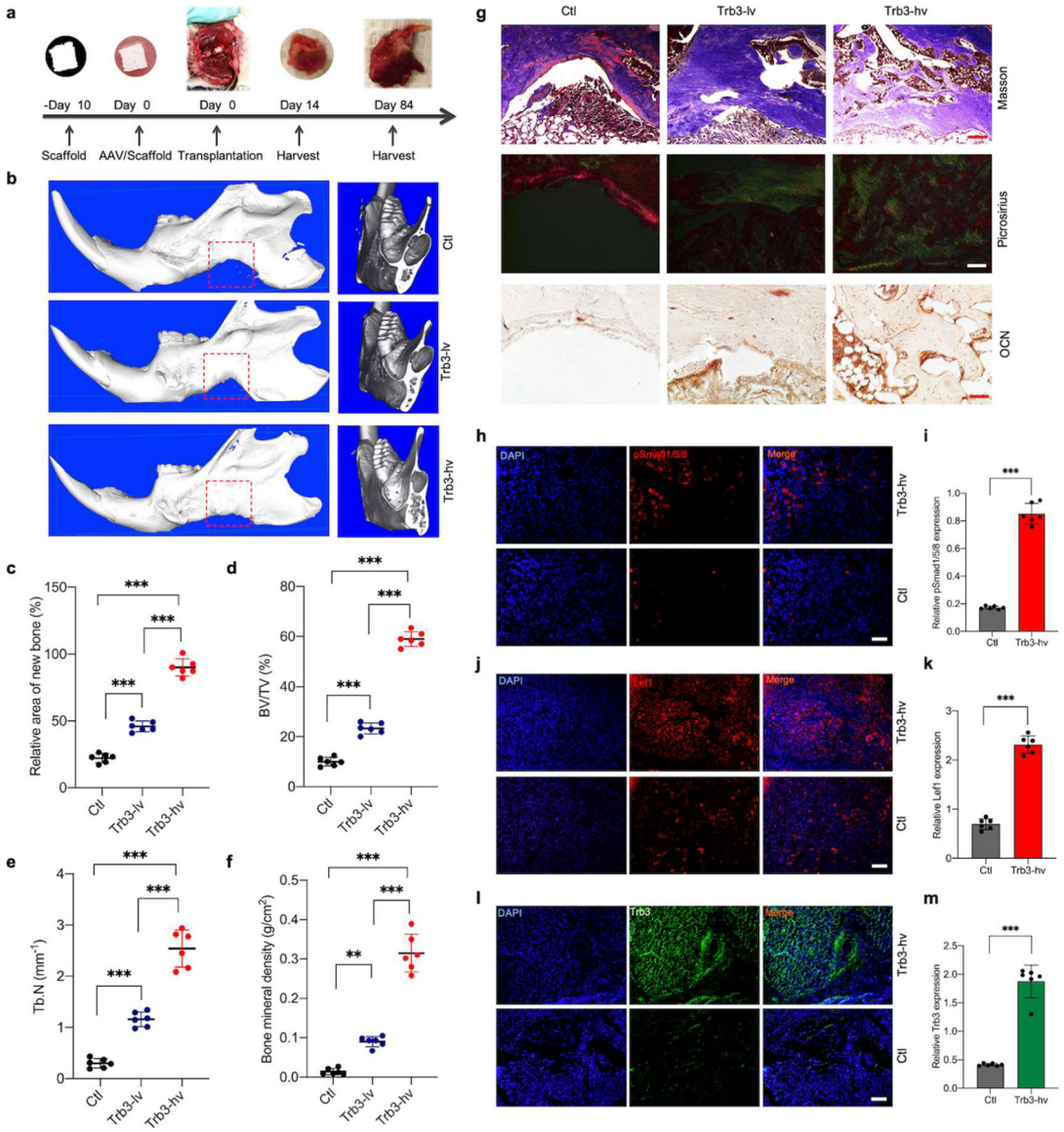

Fig. 6: Local delivery of Trb3 promotes mandibular bone regeneration *in vivo*.

(**a**): Scheme of GelCA-PLGA scaffold with AAV2-encoding Trb3 implanted into rat critical-sized (5×5 mm) mandibular defects (6 rats per group). (**b**): micro-CT images of collected graft at 12 weeks postoperatively in general (left) and sagittal sections (right). (**c–f**): Quantitative analysis of % bone surface area (c), % bone volume/tissue volume (BV/TV). (d), trabecular number (Tb.N, mm^{-1}) (e) and bone mineral density (g/cm^2) (f). (**g**): Histological analysis including Masson trichrome and Picrosirius red stain, and immunohistochemical analysis of OCN. Scale bar = 200 μm. (**h–m**): Immunofluorescence stain and colorimetric quantitation analysis of Smad4 (h,i), Lef1 (j,k) and Trb3 (l,m) in the collected implant at 2 weeks postoperatively. GelCA-PLGA, gelatin-conjugated caffeic acid coated Apatite/PLGA scaffold; Ctl, control; Trb3-lv, low dose AAV2-encoding Trb3 (2.5×10^{11} GC); Trb3-hv, high dose AAV2-encoding Trb3 (2.5×10^{12} GC). Scale bar = 200

μm. Values represent mean ± SD: $^{**}p < 0.01$ and $^{***}p < 0.001$ using a two-tailed Student's t-test and one-way ANOVA test.

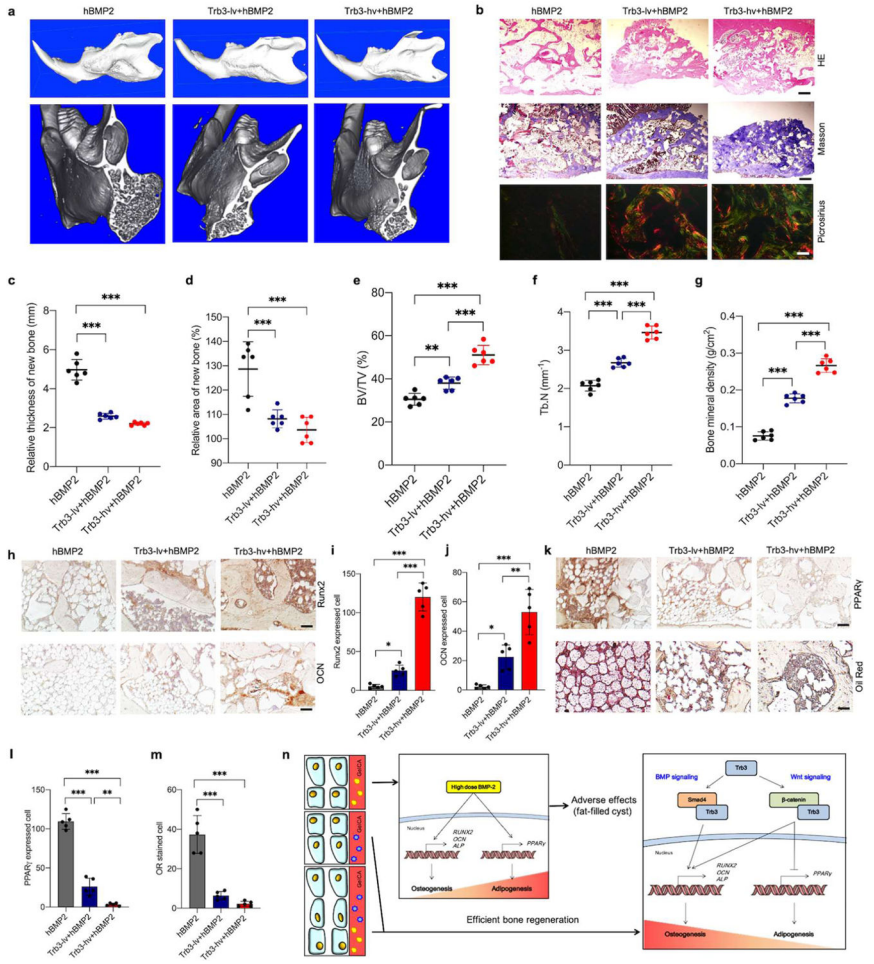

Fig. 7: *In vivo* local delivery of Trb3 enhances bone regeneration while inhibiting fat-filled cyst formation.

(**a–m**): Implantation of GelCA-PLGA scaffold loaded with AAV2-encoding Trb3 was revealed to promote bone regeneration and inhibit fat-filled cyst formation in rat critical-sized mandibular defect treated with high dose BMP2 (6 rats per group). After 12 weeks postoperatively, the collected mandibular implants were measured by the following analysis: micro-CT images (a) in general (top) and sagittal sections (below); histological analysis (b) including HE, Masson trichrome and Picrosirius stain; Quantification of thickness of new bone (mm) (c), % bone surface area (d), % bone volume/tissue volume (BV/TV) (e), trabecular number (Tb.N, mm^{-1}) (f) and bone mineral density (g/cm^2) (g); immunohistochemical stain/quantification of Runx2, OCN and PPARγ (h-l); OR stain and quantitative analysis (k,m). (**n**): Schematic diagram of Trb3-mediated pro-osteogenic and anti-adipogenic effect. Scale bar = 100 μm. GelCA-PLGA, gelatin-conjugated caffeic acid coated Ap-PLGA scaffold; hBMP2, high dose BMP2 (30 μg); Trb3-lv, low dose AAV2-encoding Trb3 (2.5×10^{11} GC); Trb3-hv, high dose AAV2-encoding Trb3 (2.5×10^{12} GC); HE, hematoxylin and eosin; OR, oil red. Values represent mean ± SD: *p < 0.05, ** p <0.01 and *** p <0.001 using one-way ANOVA test.